# Geometrical alignment properties in Fourier- and wavelet-filtered statistically stationary two-dimensional turbulence

Bartosz Protas,[1,2] Kai Schneider,[3] and Marie Farge[4]
[1]*Department of MAE, University of California, San Diego, 9500 Gilman Drive, La Jolla, California 92093-0411*
[2]*Department of Power and Aeronautical Engineering, Warsaw University of Technology, ul. Nowowiejska 24, 00-665 Warsaw, Poland*
[3]*Laboratoire de Modélisation et Simulation Numérique en Mécanique du CNRS and Centre de Mathématiques et d'Informatique, Université de Provence, 39 rue Joliot-Curie, 13453 Marseille cedex 13, France*
[4]*Laboratoire de Météorologie Dynamique du CNRS, Ecole Normale Supérieure, 24 rue Lhomond, 75231 Paris cedex 05, France*
(Received 9 May 2002; published 30 October 2002)

In this paper we compare the geometrical alignment properties of Fourier- and wavelet-filtered statistically stationary two-dimensional turbulence. The goal is to study the preferential alignment angle of vorticity gradient with respect to the compressing eigenvector of the rate-of-strain tensor, and use this quantity as a measure of how the two filtering methods affect the small scale geometric structure of the flow. The principal result is that for the case of the incoherent part obtained through wavelet filtering the probability density function of this angle is flat, meaning that this field is effectively unstructured and therefore dynamically passive. On the contrary, the corresponding field obtained through Fourier filtering reveals a bump at the angle $\pi/4$, which indicates the presence of dynamically active filament-type structures. These results provide evidence that, unlike the wavelet filtering, the Fourier filtering does remove dynamically important information from the flow.

DOI: 10.1103/PhysRevE.66.046307 PACS number(s): 47.27.Eq, 47.27.Gs, 47.11.+j

## I. INTRODUCTION

The paper addresses the issue of computing and modeling of infinite-dimensional dynamical systems when there is no spectral separability, and therefore multiscale behavior occurs. Such systems arise in many problems in continuum mechanics and, as an example, we will consider two-dimensional statistically stationary turbulence. The ultimate objective is to compute high Reynolds number flows corresponding to fully developed turbulence. Although these are dissipative phenomena, they are dominated by nonlinear dynamics, hence the number of degrees of freedom drastically increases with the Reynolds number. Even though for finite Reynolds numbers the number of degrees of freedom remains finite, it is still computationally intractable. Therefore, it is necessary to distinguish between active and passive degrees of freedom. The latter are slaved to the former in the sense that they do not exhibit their own nonlinear dynamics. The general approach is to deterministically compute the evolution of the active degrees of freedom, whereas the influence of the passive ones is only statistically modeled, as their intrinsic dynamics is essentially negligible. Hereafter we will compare two different approaches to the problem of separation of modes, namely, using the Fourier- and wavelet-filtering methods. A preliminary version of this work, including simulations at a lower resolution, appeared in Ref. [1].

## II. FOURIER AND WAVELET FILTERING

The Fourier filtering is based on the separation between low and high wave number modes and is characterized by a given cutoff wave number. This is one of the traditional filters used in large Eddy simulation (LES) to compute high Reynolds numbers flows. This classical approach relies on the assumption of scale separability of the turbulent flow dynamics. The validity of this hypothesis is still debated and in the present work we propose and analyze a different method of filtering which no longer requires this assumption. By means of nonlinear wavelet filtering (see Farge and coworkers [2–4]) we split a given flow field into a coherent and an incoherent part, corresponding to strong and weak wavelet coefficients, respectively. Both components are multiscale, but exhibit distinct statistical behaviors. For two-dimensional flows the coherent contribution corresponds to localized vortices which are characterized by a non-Gaussian vorticity probability density function (PDF) and a long range correlation. On the other hand, the incoherent contribution corresponds to a residual flow, which exhibits a Gaussian vorticity PDF and a short range correlation [3].

For two-dimensional flows the wavelet-filtering method consists in projecting the vorticity field $\omega = \partial v/\partial x - \partial u/\partial y$ ($u$ and $v$ are the two velocity components) onto a two-dimensional orthogonal wavelet basis spanned by the wavelets $\psi_\mu$, with the multiindex $\mu$ characterizing the scale, position, and direction of each basis function [2]. In this study we used the Coifman 12 wavelet which is compactly supported and has four vanishing moments. The coherent vorticity field $\omega_>$ is then reconstructed by taking only the wavelet coefficients with absolute value larger than $\tilde{\omega}_T = (4Z \ln N)^{-1/2}$. This threshold in the wavelet space depends only on the total enstrophy $Z$, which is half of the $L^2$ norm of vorticity, and on the resolution $N$, which is directly related to the Reynolds number, without any *ad hoc* adjustable parameters [3]. The choice of the threshold is motivated by statistical theorems for optimal denoising in the presence of Gaussian noise [5]. The wavelet filtering is the basis for an alternative approach to the computation of large Reynolds

 

number flows called the coherent vortex simulation (CVS) [3,6,7]. In this method the evolution of the active degrees of freedom is computed in an adaptive basis which dynamically tracks the coherent part of the flow [4,7,8]. In short, in the LES method the *resolved* components are the low wave number modes, while for the CVS method the coherent modes are *resolved* regardless of their scale. The *unresolved* parts correspond to the high wave number and the incoherent modes in the LES and CVS methods, respectively.

## III. GEOMETRICAL ALIGNMENT

The objective of the present paper is to compare the two filtering methods in terms of the structural and dynamical properties of the resolved and unresolved fields obtained as a result. It therefore constitutes a part of a larger effort wherein we seek to provide solid foundations for the CVS method. We examine the geometrical statistics (see, e.g., Ashurst *et al.* [9], Constantin [10], and Tsinober [11]) to analyze the dynamical and structural properties of the filtered fields. In the context of two-dimensional (2D) turbulence the issue of central interest is the interaction of thin, elongated filaments, produced by vortex interactions, with the strain field generated by coherent vortices. The unresolved part can be regarded as dynamically passive as long as its evolution is constrained by the resolved part. In this case the unresolved part should not exhibit its own dynamics. If, on the other hand, the background field does contain some filamentary structures then, as shown by Kevlahan and Farge [12], this field undergoes instability and may reveal dynamically significant behavior. As argued by Weiss in Ref. [13], this phenomenon is described by the equation for the evolution of vorticity gradients $\nabla\omega$ (tensor quantities are underlined),

$$\frac{d}{dt}\nabla\omega=\left(\frac{\partial}{\partial t}+\mathbf{V}\cdot\boldsymbol{\nabla}\right)\nabla\omega=-(\underline{\boldsymbol{\nabla}\mathbf{V}})^{T}\cdot\nabla\omega, \tag{1}$$

where $(\underline{\boldsymbol{\nabla}\mathbf{V}})^{T}$ denotes the transpose of the velocity gradient tensor. In the above we neglect the viscous term, as its role is only to limit the growth of vorticity gradients, whereas we are interested in the nonlinear effects associated with their stretching and folding. In Ref. [13] it was also argued that amplification of vorticity gradients is intrinsically related to the stretching term on the right-hand side of Eq. (1) and takes place in the hyperbolic (i.e., strain dominated) regions of the flow. They are characterized by the Weiss parameter $Q=s_{11}^2+s_{12}^2-\omega^2$ being greater than zero ($s_{11}=2\partial u/\partial x=-2\partial v/\partial y$ and $s_{12}=\partial u/\partial y+\partial v/\partial x$ are the strain components). Conversely, the elliptic regions of the flow, i.e., where $Q<0$, remain neutral with respect to the global dynamics of vorticity gradients. As demonstrated by Protas *et al.* in Ref. [14], the dynamics of vorticity gradients can be quantified by examining their normalized instantaneous production rate $e$ defined as

$$e=\frac{-\mathbf{m}^{T}\underline{\mathbf{S}}\mathbf{m}}{(\underline{\mathbf{S}}:\underline{\mathbf{S}})^{1/2}}, \tag{2}$$

where $\mathbf{m}=\nabla\omega/|\nabla\omega|$, and $\underline{\mathbf{S}}$ is the strain tensor, $\underline{\mathbf{S}}=\frac{1}{2}(\underline{\boldsymbol{\nabla}\mathbf{V}}+\underline{\boldsymbol{\nabla}\mathbf{V}}^{T})$. The above relation simplifies to

$$e=\frac{\sqrt{2}}{2}\cos(2\alpha), \tag{3}$$

where $\alpha$ is the angle between the vorticity gradient $\nabla\omega$ and the compressing eigenvector $\mathbf{s_2}$ of the strain tensor $\underline{\mathbf{S}}$. The above formula clarifies the relation that holds between the alignment of vorticity gradient with the principal axes of strain and the dynamics of vorticity filaments: vorticity gradients are steepened by the strain field when they lie within the range of $\pi/4$ from the principal direction of compression $\mathbf{s_2}$. An equivalent analysis can be formulated in terms of divorticity $\boldsymbol{\eta}=\boldsymbol{\nabla}\times(\omega\mathbf{k})$ which is the dual vector with respect to vorticity gradient and is always tangent to vorticity isolines. Here $\mathbf{k}$ denotes the unit vector perpendicular to the plane of motion. In this case $\alpha$ would correspond to the angle between divorticity $\boldsymbol{\eta}$ and the principal direction of stretching $\mathbf{s_1}$.

The above analysis is based on the assumption that the strain field remains frozen in time. The validity of this criterion was questioned by Basdevant and Philipovitch in Ref. [15]. However, in our investigation we perform space averages of instantaneous intensities of vorticity gradient production. Therefore, we do not have to resort to linearization in order to compute the magnitude of the nonlinear term. Consequently, the question of how long this linearization remains valid is not relevant here. The investigations of Hua, Klein, and Lapeyre (e.g., Refs. [16–18]) improve the Weiss criterion to account for temporal variation of the strain tensor.

In Ref. [14] it was shown by Protas *et al.* that the 2D forced turbulence exhibits, in the mean, preferential alignment of the vorticity gradient with the principal direction of compression $\mathbf{s_2}$. Magnitude of this alignment was shown to depend on the Reynolds number and the dissipation model (Newtonian or hyperviscous dissipation). Herein we use the same diagnostics to explore the internal structure of the vorticity fields obtained with the two different filtering methods. In the case of the Fourier filtering we consider the alignment property observed in the fields corresponding to high and low wave numbers. Similarly, for the case of the wavelet filtering we analyze the alignments in the coherent and the background part. We also provide results concerning the total field which was used for filtering.

## IV. NUMERICAL RESULTS

Here we analyze the vorticity fields obtained in a direct numerical simulation of the two-dimensional incompressible Navier-Stokes equations with periodic boundary conditions in both directions. We used a fully-dealiased pseudospectral code with constant forcing in Fourier space at the wave number $k_i=4$ and Newtonian dissipation. Due to the inverse energy cascade specific to 2D turbulent flows, we also had to add large scale dissipation in the form of Rayleigh friction (i.e., proportional to the streamfunction). Time stepping was carried out using the second order backward finite-difference scheme on the viscous terms and the Adams-Bashforth ex-

TABLE I. Comparison of the $L^2$ norms of several flow quantities and the average alignment parameters $\langle e \rangle$ for the resolved and unresolved fields obtained using the two different filters.

| Filtering method | | Number of coefficients $N$ | $E=\frac{1}{2}\int\|\vec{V}\|^2 dx$ | $Z=\frac{1}{2}\int\|\omega\|^2 dx$ | $P=\frac{1}{2}\int\|\nabla\omega\|^2 dx$ | $\langle e \rangle$ |
|---|---|---|---|---|---|---|
| Fourier | Low-pass | 0.7% | 99.4% | 90.8% | 36% | 0.16065 |
| | High-pass | 99.3% | 0.6% | 9.2% | 64% | 0.00158 |
| Wavelet | Coherent | 0.7% | 99.2% | 94.3% | 55% | 0.13316 |
| | Incoherent | 99.3% | 0.4% | 5.7% | 49% | 0.00127 |

trapolation scheme on the advection terms. Computations were performed at the resolution $N=512^2$ for time long enough to ensure that a statistically steady regime was reached (characterized by the fact that the energy spectrum no longer changes). In Table I we compare the $L^2$ norms of the relevant dynamic quantities and the field-averaged values of the alignment parameter $e$ for the Fourier and wavelet filter. In both cases we have the same fraction of retained modes, which is equal to 0.7% of the total number of modes $N$. Note that, as explained above, the averages of $e$ are restricted to hyperbolic parts of the flow domain only. One should observe that for the case of wavelet filtering the energy and palinstrophy fractions in the resolved and unresolved parts do not add up to 100%. This is due to the fact that the wavelet decomposition is orthogonal for the vorticity field, but only approximately orthogonal for its gradient and for the velocity. We observe in Table I that the wavelet filter captures more enstrophy and palinstrophy in the resolved fields than the Fourier filter. As regards the average value of the alignment parameter $e$, we find different behaviors in the resolved and unresolved fields. In the latter case the values are smaller by two orders of magnitude comparing to the total field.

Interesting information is revealed by the PDFs of the alignment angle $\alpha$ computed for the different filtered fields.

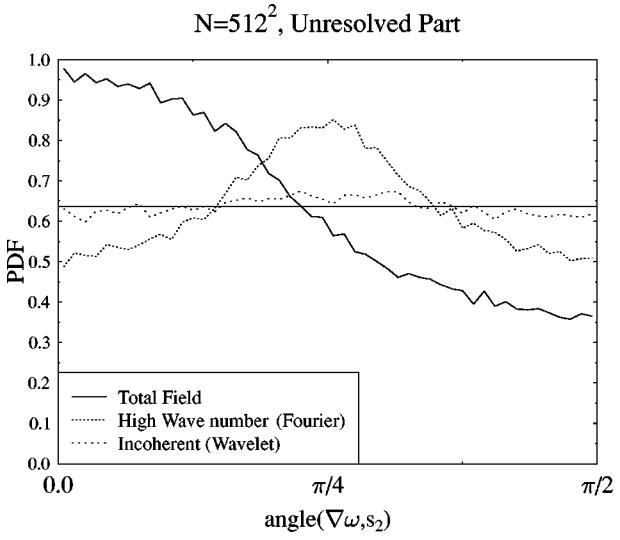


FIG. 1. PDFs of the alignment angle $\alpha$ between the vorticity gradient $\nabla\omega$ and the compressing eigenvector $\mathbf{s_2}$ for the total field, the Fourier high-pass filtered field, and the wavelet-background field.

In Fig. 1 we show the PDFs for the Fourier high-pass filtered field, the wavelet background field and, for comparison, the total field. The total field has the distribution typical for the 2D turbulent flows (cf. Ref. [14]), with large values for angles close to zero and small for angles approaching $\pi/2$. The PDF of the incoherent field is close to uniform distribution implying that this field is almost structureless. On the contrary, the Fourier high-pass filtered field reveals a distinct bump at the angle $\pi/4$. As illustrated in Fig. 2 and in the derivation presented in the Appendix, this situation corresponds, in an average sense, to the case when an isolated vorticity filament is embedded in its own strain field, and therefore the filament axis is at the angle $\pi/4$ with respect to the principal axes of strain. This provides evidence that filamentary, dynamically active structures are present in the Fourier high-pass filtered field. These observations are further corroborated by the unresolved fields shown in Fig. 3. In Fig. 3(a) we present the vorticity of the Fourier high-pass filtered field with its own compressing eigenvectors $\mathbf{s_2}$. We note that well defined, elongated structures are present and, in agreement with the data in Fig. 1, the corresponding eigenvectors form angles close to $\pi/4$ with the filaments. This confirms that the observed structures are indeed filamentary in nature. On the contrary, the unresolved field obtained from wavelet filtering is completely random and does not reveal any preferential alignment with its compressing eigenvectors. This implies that filamentary structures are absent here. As regards the resolved parts (Fig. 4), i.e., the coherent field in the case of wavelet filtering and the low-pass filtered field in the case of Fourier filtering, they both fairly well capture the PDF of the alignment angle observed for the total field. In the case of the wavelet filtering, however, the PDF is slightly underestimated.

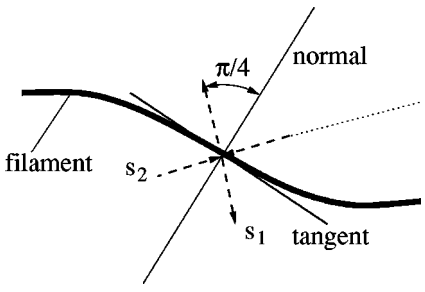


FIG. 2. Scheme showing the angle between the principal axes of strain $\mathbf{s_1}$ and $\mathbf{s_2}$ (dashed lines) and the filament with an arbitrarily shape (thick solid line).

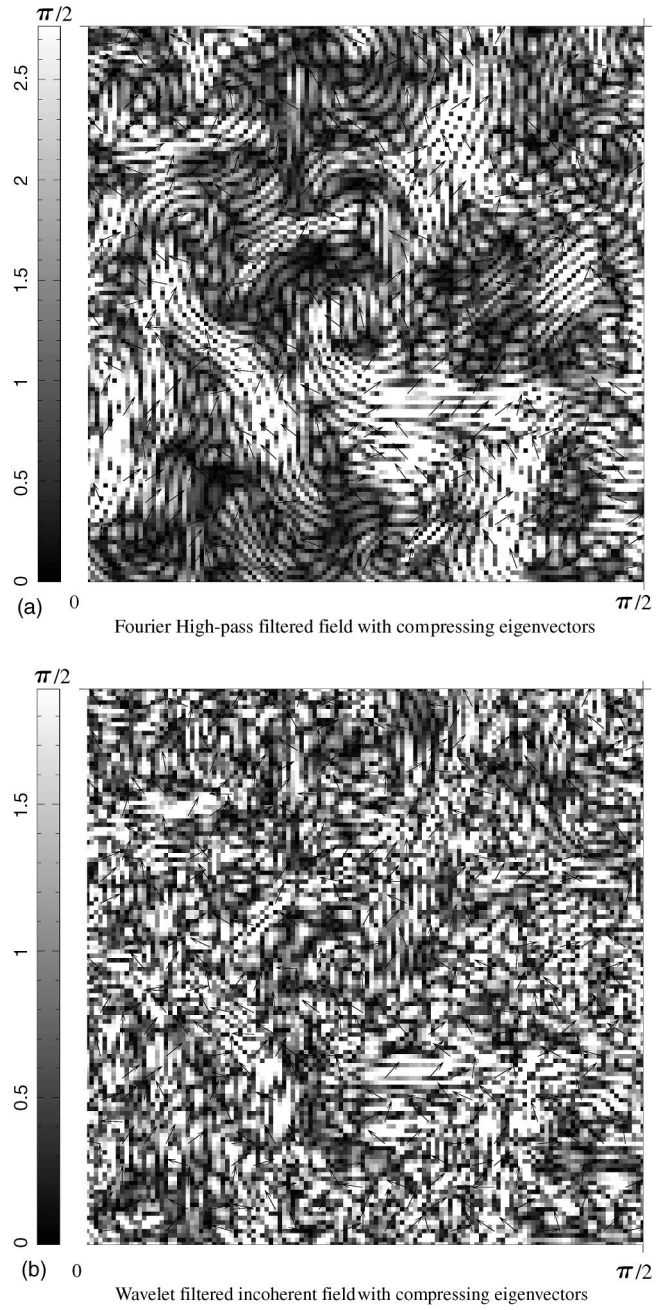


FIG. 3. Vorticity magnitude $|\omega|$ in the unresolved fields with compressing eigenvectors in hyperbolic regions. In order to magnify details, only the $[0,\pi/2]\times[0,\pi/2]$ fraction of the whole field is shown in both cases.

## V. CONCLUSION

We conclude by saying that, unlike the wavelet filtering, the Fourier filtering does remove some dynamically important information from the filtered field. It has the form of filamentary structures present in the unresolved field. Stretching and folding of such vorticity filaments is the main mechanism of the turbulent cascade in 2D flows. Consequently, the unresolved field obtained from Fourier filtering is not in statistical equilibrium and may therefore develop nontrivial behavior. Unlike the Fourier filtering, the multi-scale wavelet filtering allows one to effectively retain these nonlinear effects in the resolved fields. These findings were established using the concept of the geometrical statistics. Similar ideas were recently used by Dubos in Ref. [19] for the purpose of turbulence modeling. A natural extension of the present investigation would be to use similar diagnostics in order to study the filtering effect on 3D flows. First results concerning the wavelet filtering of 3D turbulent flows were recently reported by Farge *et al.* in Ref. [4].

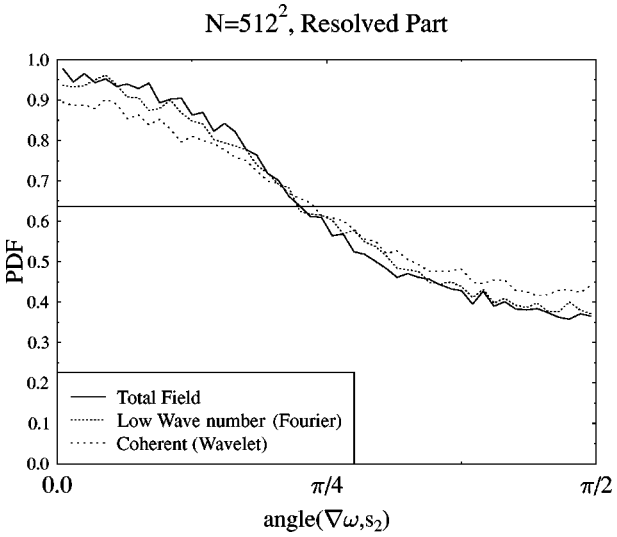


FIG. 4. PDF of the alignment angle $\alpha$ between the vorticity gradient $\nabla\omega$ and the compressing eigenvector $\mathbf{s_2}$ for the total field, the Fourier low-pass filtered field, and the wavelet-coherent field.


## ACKNOWLEDGMENTS

We thank Carsten Beta and Alexandre Azzalini for their computational support. We acknowledge partial support from the French-German Program Procope (Contract No. 99090) and the Polish-French program Polonium (Contract No. 99158).


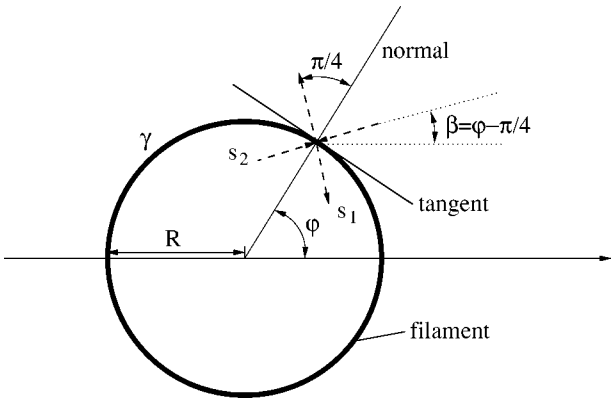


FIG. 5. Scheme showing the angle between the principal axes of strain $\mathbf{s_1}$ and $\mathbf{s_2}$ (dashed lines) and a circular filament (solid line). This configuration is related to the arbitrarily shaped filament shown in Fig. 2 through a conformal mapping.

## ACKNOWLEDGMENTS

We thank Carsten Beta and Alexandre Azzalini for their computational support. We acknowledge partial support from the French-German Program Procope (Contract No. 99090) and the Polish-French program Polonium (Contract No. 99158).


## APPENDIX

In this appendix we show that the angle between the principal axes of strain induced by a vorticity filament and the axis of this filament is equal to $\pi/4$ (this angle is the same for both stretching and compressing directions, since due to symmetry of the strain tensor, they are mutually orthogonal). In order to simplify calculations, we consider here the velocity field induced by a thin circular filament shown in Fig. 5. Using a conformal mapping (e.g., Nehari [20]), this velocity field can be transformed into the velocity field induced by a filament with an arbitrary shape (cf. Fig. 2), while preserving the angle between any two intersecting curves in the two representations. In particular, the angle between the filament axis and the principal directions of strain will be unchanged. This ensures generality of the derivation that follows. The velocity field due to the circular filament is the same as that induced by a uniform vorticity distribution within a circular disk with radius $R$ and the same total circulation $\Gamma$, and is given by

$$V(z)=(u-iv)(z)=\frac{\Gamma}{2\pi i z}, \tag{A1}$$

where $z=x+iy$ is the complex coordinate and $i$ the imaginary unit. The center of the circular filament is located at the origin. The corresponding strain field is given by

$$S(z)=\frac{1}{2}(s_{11}-is_{12})=\frac{dV}{dz}=-\frac{\Gamma}{2\pi i z^2}. \tag{A2}$$

The eigenvalues of the strain tensor $\underline{\mathbf{S}}$ are now given by $\lambda_{1/2}=\pm\sqrt{s_{11}^2+s_{12}^2}=\pm\sqrt{S(z)\overline{S(z)}}$ (overbar denotes complex conjugation) and the compressing eigenvector is $\mathbf{s_2}=[-s_{12},\lambda+s_{11}]^T=[\mathrm{Im}(S),\sqrt{S\bar{S}}+\mathrm{Re}(S)]^T$. The angle $\beta$ that this eigenvector forms with the abscissa (cf. Fig. 5) can be characterized as

$$\cot(\beta)=\frac{\sqrt{S\bar{S}}+\mathrm{Re}(S)}{\mathrm{Im}(S)}=\frac{1+\cos\left(2\varphi-\frac{\pi}{2}\right)}{\sin\left(2\varphi-\frac{\pi}{2}\right)}, \tag{A3}$$

where we used formula (A2) and $\varphi$ is the angle between the normal to the filament and the abscissa. Using now the identity $\cot(\alpha/2)=[1+\cos(\alpha)]/\sin(\alpha)$ we see that $\beta=\varphi-\pi/4$, which confirms that the compressing eigenvector forms the angle $\pi/4$ with the filament axis (and the normal to the filament). An analogous result obviously concerns the stretching eigenvector $\mathbf{s_1}$.


[1] B. Protas, K. Schneider, and M. Farge, in *Advances in Turbulence*, edited by C. Dopazo *et al.* (CIMNE, Barcelona, 2000), Vol. VIII, pp. 793–796.

[2] M. Farge, Annu. Rev. Fluid Mech. **24**, 395 (1992).

[3] M. Farge, K. Schneider, and N. Kevlahan, Phys. Fluids **11**, 2187 (1999).

[4] M. Farge, G. Pellegrino, and K. Schneider, Phys. Rev. Lett. **87**, 054501 (2001).

[5] D. Donoho and I. Johnstone, Biometrika **81**, 425 (1994).

[6] M. Farge and K. Schneider, Flow Turbul. Combust. **66**, 393 (2001).

[7] K. Schneider and M. Farge, in *Notes on Numerical Fluid Mechanics*, edited by E. H. Hirschel (Springer, New York, 2002), Vol. 82, pp. 261–270.

[8] K. Schneider, N. Kevlahan, and M. Farge, Theor. Comput. Fluid Dyn. **9**, 191 (1997).

[9] W. T Ashurst, A.R. Kerstein, R.M. Kerr, and C.H. Gibson, Phys. Fluids **30**, 2343 (1987).

[10] P. Constantin, SIAM Rev. **36**, 73 (1994).

[11] A. Tsinober, Eur. J. Mech. B/Fluids **17**, 421 (1998).

[12] N.K.R. Kevlahan and M. Farge, J. Fluid Mech. **346**, 49 (1997).

[13] J. Weiss, Physica D **48**, 273 (1991).

[14] B. Protas, A. Babiano, and N.K.-R. Kevlahan, Physica D **128**, 169 (1999).

[15] C. Basdevant and T. Philipovitch, Physica D **73**, 17 (1994).

[16] G. Lapeyre, P. Klein, and B.L. Hua, Phys. Fluids **11**, 3729 (1999).

[17] P. Klein, B.L. Hua, and G. Lapeyre, Physica D **146**, 246 (2000).

[18] G. Lapeyre, B.L. Hua, and P. Klein, Phys. Fluids **13**, 251 (2001).

[19] T. Dubos, C. R. Acad. Sci., Ser. IIb: Mec., Phys., Chim., Astron. **329**, 509 (2001).

[20] Z. Nehari, *Conformal Mapping* (McGraw-Hill, New York, 1952).